A Model for the Recovery Kinetics of Rod Phototransduction, Based on the Enzymatic Deactivation of Rhodopsin

U. Laitko and K. P. Hofmann
Institut für Medizinische Physik und Biophysik, Medizinische Fakultät Charité der Humboldt-Universität zu Berlin, D-10098 Berlin, Germany

ABSTRACT We propose a model for the recovery of the retinal rod photoresponse after a short stimulus. The approach describes the enzymatic deactivation of the photoactivated receptor, rhodopsin, by simple enzyme kinetics. An important feature of this description is that the R^* deactivation obeys different time laws, depending on the numbers of R^* formed per disc membrane and available enzyme molecules. If the enzyme works below substrate saturation, the rate of deactivation depends linearly on the number of R^*, whereas for substrate saturation a hyperbolic relation—the well-known Michaelis-Menten equation—applies. This dichotomy is used to explain experimental finding that the relation between the saturation time of the photoresponse after short illumination and the flash strength has two sharply separated branches for low and high flash intensities (up to ~10% bleaching). By relating both branches to properties of the enzymatic rhodopsin deactivation, the new model transcends the classical notion of a constant characteristic lifetime of activated rhodopsin. With parameters that are plausible in the light of the available data and the additional information that the deactivating enzyme, rhodopsin kinase, and the signaling G-protein, transducin, compete for the active receptor, the slopes of the saturation function are correctly reproduced.

INTRODUCTION

Visual signal transduction in rods starts from the absorption of photons in molecules of the photoreceptor, rhodopsin, and its transformation into an enzymatically active state. In physiological and biophysical time-resolved measurements, one uses a flash of light to activate a limited, known number of rhodopsin molecules on the disc membranes inside the rod outer segment (ROS). In the active state, rhodopsin catalyzes the formation of an active G-protein, α-transducin, which, in turn, activates phosphodiesterase, a cyclic GMP hydrolyzing enzyme. The resulting quick decline in intracellular cGMP concentration leads to the closure of cGMP-dependent ion channels in the rod cell plasma membrane, through which Ca^{2+} and Na^+ enter the cell. The blockade of the influx through channels and the continued outward flux of Ca^{2+} through a Na^+/Ca^{2+} exchanger lowers the intracellular Ca^{2+} concentration, thus leading to activation of guanylate cyclase and increased resynthesis of cGMP. In the dark resting state, the Na^+-dominated current that enters the rod through the cGMP-gated channels is balanced by an outward current through K^+ channels located in the inner segment. The interruption of this circulating current by the closure of the cGMP-gated channels, leading to a transient net outward current and hyperpolarization of the cell, is referred to as photocurrent. For a review of the role of cGMP and Ca^{2+} in visual excitation, see Pugh and Lamb (1990). For reviews of visual transduction and the enzymes involved, see Lagnado and Baylor (1992), Lamb and Pugh (1992), and Helmreich and Hofmann (1996), and for disc-membrane bound processes, see Hofmann and Heck (1996).

Although this general outline of visual transduction is well accepted, important elements remain to be clarified. This applies in particular to the recovery of the rod response, for which a satisfying and compact theory of the underlying mechanisms has not yet been proposed.

Recent electrophysiological experiments with transgenic mice impaired in rhodopsin shutoff have shown that rhodopsin deactivation is the trigger for photocurrent recovery (Chen et al., 1995). The decline of the photocurrent elicited by dim flashes in single rod cells of normal mice from its peak value of 60% of the maximum amplitude started after ~0.3 s, whereas the response of the transgenic mice was abnormally prolonged for up to 30 s. Because the mutated rhodopsin was lacking the C-terminal phosphorylation sites, the results also confirmed findings from in vitro measurements according to which a key event in the receptor deactivation was its phosphorylation, which is mediated by rhodopsin kinase (Palczewski, 1997); (Dean and Akhtar, 1996). Phosphorylation enables tight binding of arrestin (Schleicher et al., 1989), which blocks rhodopsin-transducin interaction (Wilden et al., 1986) and thereby quenches rhodopsin activity. Because the binding of kinase (Pulvermüller et al., 1993) and arrestin (Schleicher et al., 1989) is fast, the phosphorylation reactions seem to control the rate of the overall shutoff process. It is an interesting property of the rhodopsin kinase (not found with other receptor kinases; see Helmreich and Hofmann, 1996) that it competes quite effectively with transducin for binding to photoactivated rho-

Received for publication 14 August 1997 and in final form 12 November 1997.

Address reprint requests to Prof. Dr. K.P. Hofmann, Medizinische Fakultät Charité der Humbolt-Universität zu Berlin, Institut für Medizinische Physik und Biophysik, Ziegelstrasse 5-9, D-10098 Berlin, Germany. Tel.: ++49-30-2802-6141; Fax: ++49-30-2802-6377; E-mail: hofmann@rz.charite.hu-berlin.de.

0006-3495/98/02/803/13 $2.00

dopsin (Pulvermüller et al., 1993). This opens the possibility that the kinase acts as a "pre-arrestin" (Pulvermüller et al., 1993), which directly inhibits transducin activation by competition.

A simulation of the disc-localized part of the phototransduction cascade in the single quantum regime (Felber et al., 1996) has generated "effector responses" that are consistent with the electrophysiological results discussed above (Chen et al., 1995; Schneeweis and Schnapf, 1995) when a rhodopsin characteristic lifetime of 0.3 s is assumed.

With increasing flash strength, saturation was found at different stages of visual transduction. The rapid accumulation of active transducin on the disc membrane surfaces of structurally intact rod outer segments expresses itself in fast, transient changes of near-infrared light scattering (Vuong et al., 1984; Pepperberg et al., 1988). In the functioning rods of isolated retinae, the amplitude A of the scattering signal is described by $A/A_{\max} = 1 - e^{-k \cdot R^*}$, with $k \cdot R^* = 1$ occurring on the generation of approximately two R^* per disc membrane (Pepperberg et al., 1988). The conclusion from this work, namely that a large fraction of the activatable transducin pool on a membrane is affected by single photoexcitations, found strong theroretical support (Lamb, 1994; Felber et al., 1996).

The photocurrent in macaque monkey ROS was found to saturate with amplitudes of up to 34 pA; the experimentally determined response-stimulus relation between photocurrent and flash strength is again fitted by an exponential function of the form $I/I_{\max} = 1 - e^{-k \cdot R^*}$, with $k \cdot R^* = 1$ at ~43 R^* per ROS (Baylor et al., 1984). The state of photocurrent saturation is characterized by complete closure of all cGMP-dependent channels, an essentially zero level of intracellular cGMP, and essentially maximum guanylate cyclase activity. When photocurrent saturation is reached, further increase in flash strength does not evoke a stronger response, but a prolonged saturation period that precedes the onset of the recovery. Measurements by Birch, Pepperberg, and co-workers (Birch et al., 1995; Pepperberg et al., 1996) determined the apparent photocurrent saturation time from the delayed recovery of the human rod electroretinogram *a* wave after a flash. The data points in Fig. 1 are the result of their experimental work and represent the relation between the saturation time T (the period after the test flash during which a second flash does not generate a noticeable *a* wave) and the natural logarithm of the rhodopsin amount produced by the test flash. Here and in previous work (Pepperberg et al., 1992), the slope of this "saturation function" was identified with the characteristic lifetime of a component of the visual transduction cascade that determines the time the effector activity in the ROS needs to decline to a certain "criterion level" and thereby the length of the saturation period. It is obvious from Fig. 1 that the saturation function is biphasic. A similar result was also obtained from ERG of murine retinae (Lyubarsky and Pugh, 1996) and, recently, from photocurrent experiments on single monkey rod cells (D. Schneeweis, personal communication). The conclusion drawn by Pepperberg et al. from the two-branched nature of the saturation function was that, for weak and strong bleaches, the lifetimes of two different components of the transduction cascade determine the saturation time. They identified these components with the effector itself for weak bleaches and active rhodopsin for strong bleaches. To uncouple the effector decline from the rhodopsin action for weak bleaches, they assumed a long-lived refractory state of the effector. Comparison of their model with the experimental data in Fig. 1 yielded an R^* characteristic lifetime of 2.3 s, together with an effector lifetime of 0.3 s and a lifetime of the refractory state of 6.7 s. The basics of their model, specifically the description of the excitability of the ROS as a sum of unit events, each triggered by the presence of at least one R^* in the related unit event area, and the Poisson distribution of the R^* among the unit event areas, are adopted here.

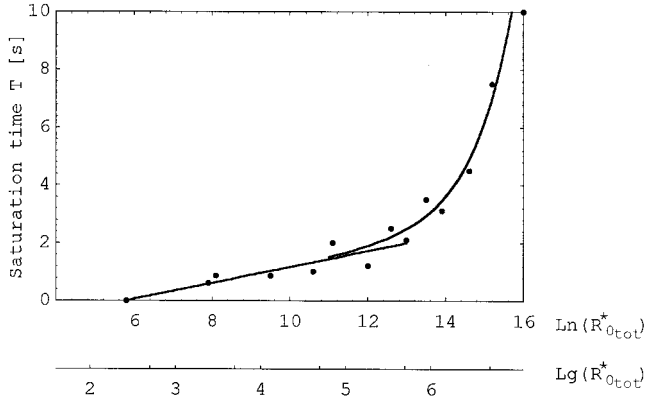

FIGURE 1 Data points of the experimentally determined saturation function (Pepperberg et al., 1996; Birch et al., 1995), where T is the length of the saturation period and $\ln(R^*_{0_{tot}})$ is the natural logarithm of the number of activated rhodopsin molecules generated in the ROS by a test flash. The curves represent the expressions for the two branches of the saturation function. as given by the model in Eqs. 22 and 23 with the following parameters: $k_1 = 0.0066\ s^{-1}\ n^{-1}$; $k_2 = 1\ s^{-1}$; $RK_{tot} = 600$ n; $N = 1500$.

The description of rhodopsin decay by first-order kinetics, i.e., as an exponential function with a certain characteristic time over the entire spectrum of bleachings, as it was used by Pepperberg et al., (1996) and in other previous attempts at mathematical modeling of transduction deactivation kinetics (e.g., Felber et al., 1996), is the simplest possible approach. Considering the enzymatic and multistep nature of this process, it is not really satisfying and definitely loses validity if it comes to substrate saturation of the involved enzymes. The rhodopsin kinase content of a vertebrate ROS is 0.5–2.0% of the rhodopsin content (K. Palczewski, personal communication). Together with the fast and efficient binding of rhodopsin kinase, as determined in vitro ($k_{on} = 1\ \mu M^{-1}\ s^{-1}$, $K_D = 0.3$–$0.5\ \mu M$; Pulvermüller et al., 1993), this suggests that already small bleaches of no more than 1% should suffice to put rhodopsin kinase into the substrate-saturated state. To account for this, we used a simple two-step enzymatic process as a model for rhodopsin shutoff. It is still simplified, but the reduction of the shutoff to the interaction between rhodopsin and its kinase can be

justified by the short time it takes to bind arrestin once R^* is phosphorylated (Schleicher et al., 1989; Pulvermüller et al., 1997). The model exhibits a dependence of behavior on the initially generated amount of active rhodopsin, which explains some of the above-mentioned experimental findings in a straightforward way.

THE MODEL

Effector activation on a disc membrane

The formation of activated rhodopsin R^* on a disc membrane results in a quick rise in effector (active phosphodiesterase) activity E. If R^* persists long enough, the effector activity will reach a plateau E_{max} that is characterized by steady reactivation of effector that returns from the active/refractory state. The upper limit for this plateau activation is the total number of effectors on a disc. Light-scattering measurements on bovine ROS (Pepperberg et al., 1988) suggested that near-maximum effector activity on a disc is reached at a generation of two R^*. Stochastic simulations of the transduction processes on a disc membrane (Felber et al., 1996) confirm these findings. Fig. 2 shows effector activity versus time as it was found in these stochastic simulations for various numbers of persisting R^*. The legend to this figure gives a short account of the rate constants assumed for the partial reactions. Justified by these data, we may understand the disc membrane as the location of two possible unit events, where a unit event, characterized by a half-maximum effector plateau activity E_{max}, is triggered by the formation of one R^*. For the sake of simplicity and on the time scale of seconds, we may assume that the maximum unit event activity $E_{max}/2$ is immediately reached and maintained as long as there is at least one R^* present.

Fig. 3 illustrates this simple model for the disc-localized part of phototransduction. R^* is formed by a flash and undergoes catalytic deactivation. The transducin GTPase cycle on the disc membranes is condensed into activation of G_t, subsequent formation of active effector by complex formation between G_t and phosphodiesterase, and reformation of the inactive G_t either directly or via a refractory period.

Rhodopsin deactivation on a disc membrane

Fig. 3 contains the scheme of a simple irreversible enzyme reaction for the R^* phosphorylation by rhodopsin kinase (RK). Formation of the enzyme substrate complex R^*RK is followed by phosphorylation and product release. The phosphate donor, ATP, is assumed to be very well buffered, so it is included in the kinetic constant, and the second and third steps are lumped into one in our calculations. By applying this scheme, we employ a standardized rhodopsin shutoff mechanism (with an unspecified number of phosphate groups involved), where one phosphorylation step causes both RK release and rapid deactivation of R^* via arrestin binding. According to Pulvermüller et al. (1993), phosphorylated rhodopsin shows only weak if any binding to the kinase, so the available experimental evidence is consistent with this assumption. For the sake of simplicity, we assume that RK is constantly active, at least until all of the R^* formed is deactivated. This embraces the "hysteresis" and "stable complex" models of RK function, as long as

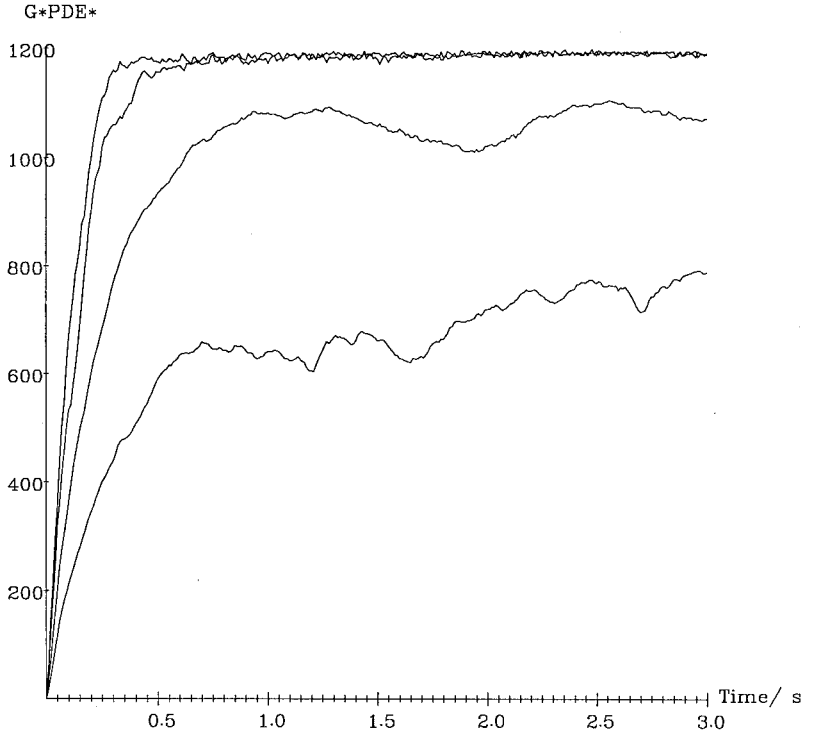

FIGURE 2 Simulated phosphodiesterase activity on a model disc membrane for various numbers of long-lived (persisting) R^*. $R^* = 1, 2, 3, 4$ for the curves from bottom to top. The first and second curves are averaged over 10 realizations. The figure shows that it is justified to assume that one R^* on a disc maintains the half-maximum effector activity. For the partial steps of the transducin GTPase cycle, the following parameters were used in the stochastic simulations: 3 s^{-1} n^{-1} for the complex formation between R^* and G_t; 8000 s^{-1} for the release of activated transducin; 0.05 s^{-1} for the transition of active G_t into the refractory state; 0.3 s^{-1} n^{-1} for the binding of $G_{t\alpha}$ to PDE; 2 s^{-1} for the decay of the $G_{t\alpha}$-PDE complex; 2 s^{-1} for the reformation of activatable transducin from the refractory state. For details of the method, see Felber et al. (1996).

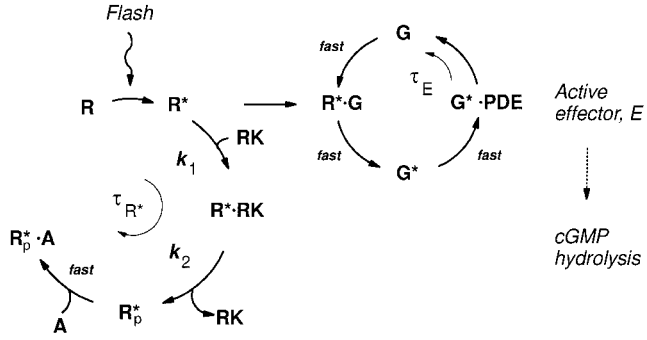

FIGURE 3 Reaction scheme of a simple model for the disc-localized part of visual transduction. Photoactivated rhodopsin R^* converts transducin G to G*; G* combines with phosphodiesterase PDE to form the active, cGMP-hydrolyzing effector, which decays with a certain characteristic lifetime τ_E. R^* itself is deactivated via binding of and phosphorylation by the enzyme rhodopsin kinase *RK* and subsequent fast binding of arrestin A. In the model, it is assumed that a steady state of the transducin-coupled processes is reached well within the lifetime of R^*, τ_{R^*}.

the R^* phosphorylation event terminates the lifetime of a given R^*RK complex. We do not consider phosphorylation of inactive rhodopsin or shut-off of *RK* by autophosphorylation within the relevant time domain. For a review of these biochemical aspects, see Palczewski (1997).

Because the R^* phosphorylation happens on disc membranes with numbers of the involved molecules on the order of mere tens, hundreds, or thousands, a rigorous treatment of the system kinetics must consider probabilities of reactions rather than reaction rates (Felber et al., 1996; Lamb, 1994); stochastics of particle numbers—rather than concentrations—come into play. The kinetic equations and their solutions describe the temporal evolution of expectation values of a stochastic process. We will come back to this point below.

However, let us first introduce the kinetic equations for the enzymatic R^* deactivation in a straightforward form:

$$\begin{aligned}\frac{dR^*}{dt} &= -k_1 \cdot (RK_{tot} - R^*RK) \cdot R^* \\ \frac{dR^*RK}{dt} &= k_1 \cdot (RK_{tot} - R^*RK) \cdot R^* - k_2 \cdot R^*RK\end{aligned} \tag{1a}$$

where R^* and R^*RK are the amounts of the respective species at time t with initial conditions

$$\begin{aligned}R^*(0) &= R_0^* \\ R^*RK(0) &= 0\end{aligned} \tag{1b}$$

The conservation of the total enzyme amount RK_{tot} was used to eliminate the free enzyme *RK* as a variable in Eq. 1a. k_1 denotes the bimolecular kinetic constant for the association of R^* and RK, and k_2 is the monomolecular kinetic constant for product release.

We may now consider two limiting cases. Large or small values of the ratio φ of total enzyme amount and initial R^*,

$$\varphi = \frac{RK_{tot}}{R_0^*} \tag{2}$$

allow certain simplifications of the kinetic equations. In the first case, if R_0^* is much smaller than RK_{tot}, the reduction of the free enzyme amount by the number of enzyme molecules that are engaged in the enzyme substrate complex can be neglected. Thus approximation of the R^* decay by first-order kinetics is allowed:

$$\left.\frac{dR^*}{dt}\right|_{\varphi \gg 1} \approx -k_1 \cdot RK_{tot} \cdot R^* \tag{3}$$

For initial amounts of R^* that significantly exceed the total enzyme amount, a quasi-steady-state approximation for R^*RK can be used. The application of this well-known method to reduce the complexity of systems of differential equations is explained for this special case in Appendix A. It results in the hyperbolic relation

$$\left.\frac{dR^*}{dt}\right|_{\varphi \ll 1} \approx -\frac{k_2 \cdot RK_{tot} \cdot R^*}{k_2/k_1 + R^*} \tag{4}$$

Both approximations provide solutions for $R^*(t)$. Equation 3 results in

$$R^*(t)|_{\varphi \gg 1} = R_0^* \cdot e^{-k_1 \cdot RK_{tot} \cdot t} \tag{5}$$

Equation 4 yields a solution for $R^*(t)$ that is implicitly given by

$$\begin{aligned}t|_{\varphi \ll 1} = &\frac{1}{k_1 \cdot RK_{tot}} \cdot (\ln R_0^* - \ln R^*(t)) \\ &+ \frac{1}{k_2 \cdot RK_{tot}} (R_0^* - R^*(t))\end{aligned} \tag{6}$$

Fig. 4 compares the approximations in Eqs. 5 and 6 with the numerical integration of Eq. 1 for different values of R_0^*. Especially in the late phase of R^* deactivation (i.e., for small $R^*(t)$), which is crucial for the departure from saturation, both approximations within their respective bounds of validity reproduce the actual time course of R^* satisfyingly well.

Distribution of R* among the disc membranes

To account for the compartimentalized nature of the rod outer segment, it is necessary to consider the distribution of R^* among disc membranes. For flash strengths that generate multiple R^*, the distribution of the initially generated $R^*_{0,tot}$ active rhodopsin molecules among the N disc membranes of the ROS may be considered Poissonian with an expectation value r_0^* for the number of R^* initially found on one disc membrane of

$$r_0^* = \frac{R^*_{0_{tot}}}{N} \tag{7}$$

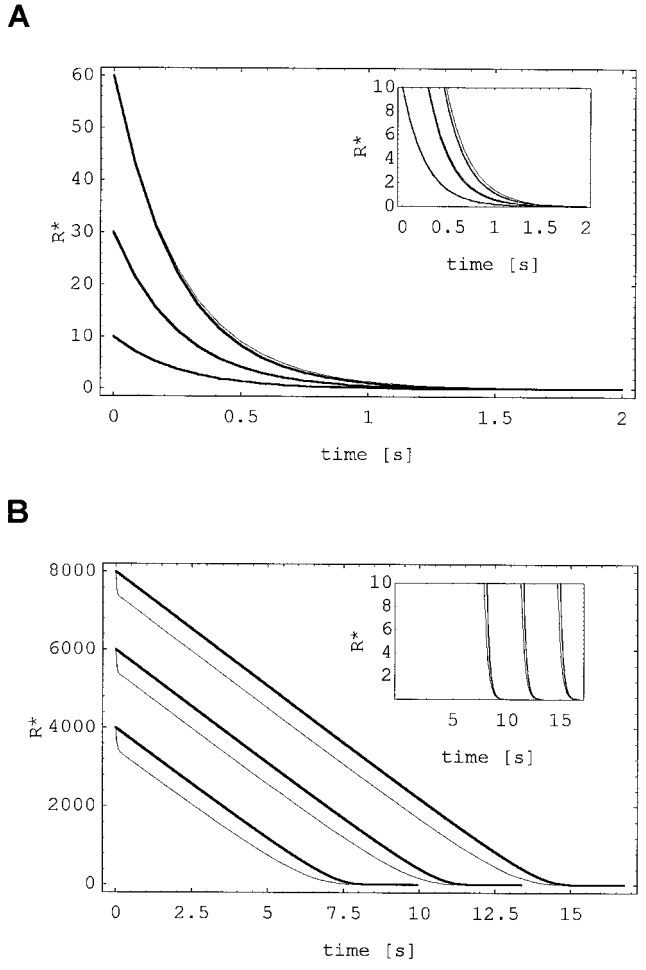

FIGURE 4 Approximative versus exact numerical solution of the kinetic equations in Eq. 1 for weak and strong flashes. The insets magnify the tail of both curve sets. The thin lines represent a numerical integration of the differential equations system in Eq. 1. Parameters are as in Fig. 1. (*A*) Approximation for weak flashes (Eq. 5) (*thick lines*) compared with the numerical integration of Eq. 1 for $R_0^* = 10, 30, 60$. (*B*) Approximation for strong flashes (Eq. 6) (*thick lines*) compared with the numerical integration of Eq. 1 for $R_0^* = 4000, 6000, 8000$.

and

$$P_k(0) = \frac{r_0^{*k}}{k!} \cdot e^{-r_0^*} \tag{8}$$

for the probability to find k R^* on one disc membrane at time 0. At later times, the number of R^* reduces separately on each disc membrane, according to the enzymatic scenario that was outlined in the previous section. The temporal evolution of the probability distribution is governed by a master equation:

$$\frac{dP_k(t)}{dt} = P_{k+1}(t) \cdot f(k+1) - P_k(t) \cdot f(k) \tag{9}$$

with the initial conditions given by Eq. 8 for each $k \in [0, R^*_{0_{tot}}]$. (There is no gain of probability from the $(k-1)$ state, because the number of R^* on a disc can only decline.) The transition rates $f(k)$ denote the rate at which a disc membrane that contains k R^* transforms into one that contains $(k-1)$ R^*. They are related to the kinetic equations in Eq. 1.

Because the character of the initial distribution of the R^* among the disc membranes might be changed by the R^* decay, the question arises whether, during the process described by Eq. 9, the Poissonian character of the probability distribution for the number of R^* on a disc membrane retains. This means, specifically: Does

$$P_k(t) = \frac{r^*(t)^k}{k!} \cdot e^{-r(t)} \tag{10}$$

hold for all t?

In Appendix B, a condition for conservation of the Poisson distribution is derived. Appendix C relates the transition rates f to the kinetics of the enzymatic R^* decay and introduces approximations for large and small values of the stochastic analogon of Eq. 2, the characteristic initial ratio

$$\bar{\varphi} = \frac{RK_{tot}}{r_0^*} \tag{11}$$

It is no surprise that these approximations are again the stochastic analoga of the deterministic kinetic equations Eqs. 3 and 4:

$$f(k)|_{\bar{\varphi} \gg 1} \approx k_1 \cdot RK_{tot} \cdot k \tag{12}$$

$$f(k)|_{\bar{\varphi} \gg 1} \approx \frac{k_2 \cdot RK_{tot}}{k_2/k_1 + r^*(t)} \cdot k \tag{13}$$

(Note the occurrence of the expectation value $r^*(t)$ instead of the stochastic variable k itself in the denominator of Eq. 13, which makes the transition rate linear in k.) In Appendix D it is confirmed that the estimations of the rate at which the expectation value $r^*(t)$ changes that result from the stochastic approach are indeed identical to the deterministic kinetic Eqs. 3 and 4 for large (resp. small) values of $\bar{\varphi}$.

Thus we have shown that the Poissonian character of the distribution of the R^* among the disc membranes is conserved for weak and strong flashes, i.e., Eq. 10 holds for all t if $\bar{\varphi}$ in Eq. 11 is either large or small.

For intermediate flashes that generate R^* quantities on the order of the RK content on each disc, analytical treatment of the differential equations for the deterministic R^* kinetics in Eq. 1 or the differential equations for the temporal evolution of the probability distribution $P_k(t)$, Eqs. C3 and C4, is impossible. Therefore we will limit our further examinations to weak and strong flashes. However, it is reasonable to assume that the solution for intermediate flashes will be a continuous transition between these two limiting cases.

Time course of effector activation for weak and strong flashes

As elaborated above (Effector Activation on a Disc Membrane), we assume that a disc membrane is the location of

two possible unit events, i.e., one R^* maintains a plateau $E_{max}/2$, two or more R^* maintain a plateau E_{max} on the disc. According to the Poisson distribution given by Eq. 10 of R^* among the disc membranes, the probabilities to have one or, respectively, at least two R^* on a disc membrane at time t are

$$P_{k=1}(t) = r^*(t) \cdot e^{-r^*(t)}$$
$$P_{k>=2}(t) = 1 - (r^*(t) + 1) \cdot e^{-r^*(t)} \quad (14)$$

These probabilities determine the fractions of the N disc membranes that contribute with $E_{max}/2$ (resp. E_{max}) to the overall ROS effector activity. The resulting normalized activity at time t for the entire ROS is

$$\frac{E_{tot}(t)}{E_{max} \cdot N} = 1 - (1 + r^*(t)/2) \cdot e^{-r^*(t)} \quad (15)$$

where $E_{max} \cdot N$ is the maximum effector activity in the ROS. For small $r^*(t)$, Eq. 15 can be well approximated by

$$\frac{E_{tot}(t)}{E_{max} \cdot N} = 1 - e^{-r^*(t)/2} \quad (15a)$$

the function for the saturation of the light scattering signal (ATR) amplitude that was experimentally found by Pepperberg et al. (1988). Equation 15a is the probability of finding at least one R^* on a disc membrane for a system with $2N$ disc membranes. This means that for small $r^*(t)$, the two halves of a disc membrane, each being the localization of a unit event, may be treated independently.

The expectation value kinetics that enter Eqs. 15 and 15a are different for weak and strong flashes. For weak flashes, Eq. 5 gives the analytical solution for $r^*(t)$ directly, whereas for strong flashes the solution applies that is implicitly contained in Eq. 6. Fig. 5 shows the time course of the normalized effector activity for weak and strong flashes that generate different initial expectation values r_0^*.

The course of effector activity must not be confused with that of the circulating current it causes. The only property of the circulating current response that can be directly derived from the effector response via the reach of a criterion level is the time of its departure from saturation (Pepperberg et al., 1996). Such an analysis will be presented in the following section. cGMP hydrolysis by the effector, cooperative binding of cGMP to the channels, the Ca^{2+} dependency of guanylate cyclase, and the influence of the other ion concentrations in the rod cell cytoplasm, which will presumably deviate from their dark resting state values after a period of photocurrent saturation, introduce much nonlinearity in the relation between effector and current. Thus experimental findings of a progredient overall slowing of the circulating current recovery from saturation with progressive increases in flash strength (Pepperberg et al., 1992) may well be compatible with the translation invariance of the effector recovery shapes in Fig. 5.

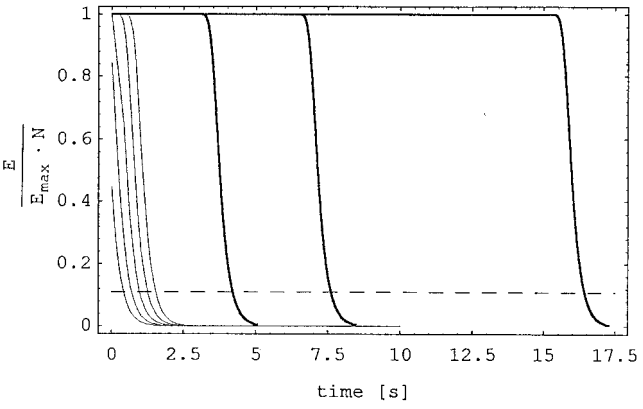

FIGURE 5 Two sets of curves representing the time course of normalized effector activity in the ROS for weak and strong flashes: $r_0^* = 1$, e, e^2, e^3, e^4 (*thin lines*); $r_0^* = e^7$, e^8, e^9 (*thick lines*). A measure of flash intensity is the parameter $\bar{\varphi}$ (Eq. 11); see text for details. Subsequent curves of each set are characterized by e-fold increases in the initial expectation value for the rhodopsin content of a disc membrane, r_0^*. The broken horizontal line stands for the criterion level of effector activity as determined from the r_0^* value at the intersection of the experimental saturation function with the time axis and Eq. 16. Parameters are as in Fig. 1.

COMPARISON OF THE RESULTS OF THE MODEL WITH EXPERIMENTAL DATA

We come back to Fig. 1, which plots the time T of photocurrent saturation after a test flash against the logarithm of the initial active rhodopsin $R^*_{0_{tot}}$ generated by that flash in the ROS. These data were obtained from the recovery of the human rod ERG *a* wave in paired-flash experiments by Pepperberg et al. (1996). They referred to that relation as saturation function and suggested that the saturation time was the time it takes for the effector (phosphodiesterase) activity in the ROS to decline to a certain criterion level, which is characterized by the momentary balance between the declining effector concentration and the essentially constant maximum guanylate cyclase concentration that is maintained during photocurrent saturation. Beyond that point, the cGMP starts to recover from its essentially zero level, and a second flash can evoke a response.

According to this, and with Eq. 15 for the normalized effector activity, for all points of the saturation function,

$$C = 1 - (1 + r^*(T)/2) \cdot e^{-r^*(T)} \quad (16)$$

has to be fulfilled. C denotes the normalized criterion level of effector activation in the ROS. The relation between $r^*(T)$ and $\ln R^*_{0_{tot}}$ on the abscissa of Fig. 1 is given by

$$r_0^* = \frac{R^*_{0_{tot}}}{N} \text{ and } r^*(T) = f(r_0^*, T) \quad (17)$$

The constant C can be determined from the coordinates of the intersection of the saturation function with the x axis, because at that point, with $T = 0$,

$$r^*(T) = r_0^* = \frac{R^*_{0_{tot}}}{N} \quad (18)$$

is valid. We denote

$$r^*_0|_{T=0} = \bar{r}^*_0 \text{ and } R^*_{0_{tot}}|_{T=0} = \bar{R}^*_{0_{tot}} \tag{19}$$

From Eq. 16 and from the determination of the constant C by Eq. 18, it follows that for all points of the saturation function,

$$r^*(T) = \bar{r}^*_0 \tag{20}$$

must be valid, i.e., $r^*(T)$ in Eq. 20 is the expectation value for R^* that maintains the criterion level C of effector activity in the ROS. In Fig. 5, C is denoted by the broken horizontal line. Subsequent curves of one set in the figure represent the course of $r^*(t)$ for e-fold increases in r^*_0. Thus the space between the intersections of the curves with the criterion line, i.e., the additional time it takes for the ROS effector activity to decline to the criterion level after an e-fold increase in r^*_0, is the slope of the saturation function. The figure shows that the slope is constant for weak flashes, and it continuously increases for strong flashes.

With Eqs. 16 and 5, we have for the branch of the saturation function that is related to weak flashes,

$$C = 1 - \exp[-r^*_0 \cdot \exp[-k_1 \cdot RK_{tot} \cdot T]] \cdot \left(1 + \frac{r^*_0}{2} \cdot \exp[-k_1 \cdot RK_{tot} \cdot T]\right) \tag{21}$$

$$\text{or} \quad \bar{r}^*_0 = r^*_0 \cdot e^{-k_1 \cdot RK_{tot} \cdot T}$$

hence

$$T|_{\bar{\varphi} \gg 1} = \frac{1}{k_1 \cdot RK_{tot}} \cdot \ln \frac{r^*_0}{\bar{r}^*_0} = \frac{1}{k_1 \cdot RK_{tot}} \cdot \ln \frac{R^*_{0_{tot}}}{\bar{R}^*_{0_{tot}}} \tag{22}$$

with the use of Eq. 17.

The model predicts a linear slope for T versus $\ln R^*_{0_{tot}}$ for weak flashes. This behavior depends crucially on the exponential relation in Eq. 15, which resulted from the Poissonian distribution of R^* among compartments (Pepperberg et al., 1996).

For the branch of the saturation function that is related to strong flashes, we find with Eqs. 16, 20, and 6,

$$\begin{aligned} T|_{\bar{\varphi} \ll 1} &= \frac{1}{k_1 \cdot RK_{tot}} \cdot \ln \frac{r^*_0}{\bar{r}^*_0} + \frac{r^*_0 - \bar{r}^*_0}{k_2 \cdot RK_{tot}} \\ &= \frac{1}{k_1 \cdot RK_{tot}} \cdot \ln \frac{R^*_{0_{tot}}}{\bar{R}^*_{0_{tot}}} + \frac{R^*_{0_{tot}} - \bar{R}^*_{0_{tot}}}{N \cdot k_2 \cdot RK_{tot}} \end{aligned} \tag{23}$$

Fig. 1 shows the functions given by Eqs. 22 and 23 with $k_1 = 0.0066\ s^{-1}\ n^{-1}$, $k_2 = 1\ s^{-1}$, $RK_{tot} = 600$, and $N = 1500$, and the data points of the experimentally determined saturation function.

Our theory started from known properties of the rod photoreceptor, namely the disc membrane structure and the enzymatic nature of R^* deactivation. The comparison with the ERG data, based on kinetic properties of rhodopsin kinase, provides a test for the validity of the model. Values for RK_{tot} and k_2 are relatively well established, namely $RK_{tot} \approx 0.4$–2% of rhodopsin, that means 12–60 μM or ~300–1200 molecules per disc membrane, and $k_2 \approx 1\ s^{-1}$ (K. Palczewski, personal communication). Parameter values in this range, together with the bimolecular constant k_1 for membrane-bound R^*-RK interaction assumed to be $\sim 0.0066\ s^{-1}\ n^{-1}$, reproduced the saturation function well. For a comparison of k_1 with the experimental k_{on} (0.5–1 $\mu M^{-1}\ s^{-1}$, leading to a formally extrapolated time of binding of RK to R^* of <170 ms), one has to be aware that 1) the k_{on} was obtained for low concentrations of solubilized RK (0.5–1.5 μM); RK in its native state and in physiological concentrations may well behave differently, as was already pointed out by Pulvermüller et al. (1993); 2) there is evidence that RK may bind to R^* from a disc-membrane-associated state (Helmreich and Hofmann, 1996; Inglese et al., 1993). If that is the case, the native binding of RK to R^* would be a membrane-located, two-dimensional process, whose kinetic parameters cannot be directly compared to those determined for a three-dimensional process, as is the binding of RK to R^* from solution.

The time of binding of RK to R^* as estimated by the model is on the order of 250 ms. The bimolecular kinetic constant is given in units of "per second and particle number," because our calculations where performed for numbers of particles instead of concentrations. For a formal transformation into concentration units, the reaction volume is required. It may be roughly approximated as $1/N$ of the ROS cytoplasmatic volume (see Table 1), which gives a value of k_1 on the order of 0.1 $s^{-1}\ \mu M^{-1}$.

INFLUENCE OF THE EXPONENTIAL DECAY OF EFFECTOR ACTIVITY AFTER COMPLETE R* DEACTIVATION ON THE DISCS

So far it was assumed for the sake of simplicity that the effector activity on a disc membrane immediately returns to zero if all R^* is deactivated. Thus the contribution of these "empty" disc membranes to the overall effector activity was neglected. Now we are going to estimate the influence that the more realistic assumption of exponential decay of the effector activity has on the propositions of our model.

To facilitate our estimation, we employ the approximation from Eq. 15a and treat the ROS as if it had $2N$ independent disc membranes, each with a maximum effector activity $E_{max}/2$. At time t, the effector activity on a disc membrane whose last active R^* was deactivated at time τ has declined from its maximum value down to

$$E(t, \tau) = \frac{E_{max}}{2} \cdot e^{-(t-\tau)/\tau_E} \tag{24}$$

At time τ, the number of disc membranes that lose their last R^* is then

$$2 \cdot N \cdot dP_{R^*=0}(\tau) = -N \cdot \frac{dr^*(\tau)}{dt} \cdot e^{-r^*(\tau)/2} \cdot d\tau \tag{25}$$

TABLE 1 Abbreviations, symbols, and typical values of parameters that enter the model

	Abbreviation	Typical values in vertebrate rod cells
Rod outer segment	ROS	Cytoplasmatic volume ~30 μm^3
Number of disc membranes per ROS	N	1000–2000
Rhodopsin	R	~3 mM or ~50,000 molecules/disc membrane
Photoactivated rhodopsin/expectation value for the number of photoactivated rhodopsins per disc membrane	R^*/r^*	Up to ~9000 molecules/disc membrane in the experiments of Fig. 1
Rhodopsin kinase content per disc membrane	RK_{tot}	12–60 μM or 300–1200 molecules/disc membrane*
(Maximum) Effector activity on a disc membrane	E, E_{max}	~600 molecules/disc membrane[#]
Bimolecular kinetic constant of RK binding to R*	k_1	~0.5–1 s^{-1} μM^{-1}[§]
Monomolecular constant of R* phosphorylation and release	k_2	~1 s^{-1}[1]

*K. Palczewski (personal communication).
[#]Hofmann and Heck (1996).
[§]Pulvermüller et al. (1993).

Equations 24 and 25 together give us the residual effector activity contribution from these disc membranes at time t:

$$E^+(t, \tau) = 2 \cdot N \cdot dP_{R^*=0}(\tau) \cdot E(t, \tau) \quad (26)$$

The contribution of the residual effector activity on all disc membranes that have lost their last R^* in the time interval $(0, t)$ at time t is the sum of Eq. 26 over all times τ, i.e., the integral

$$E^+(t) = \int_0^t 2 \cdot N \cdot dP_{R^*=0}(\tau) \cdot E(t, \tau) \quad (27)$$

Appendix E shows how Eq. 27 can be solved for the case of first-order kinetics of rhodopsin decay. The overall effector activity in the ROS at time t is now

$$E_{tot}(t) = E(t) + E^+(t) \quad (28)$$

with $E(t)$ as in Eq. 15a. Fig. 6 compares the overall effector activity with and without consideration of $E^+(t)$, as given by Eqs. 15 and 28 for weak flashes (i.e., exponential R^* deactivation, $\tau_{R^*} = k_1 \cdot RK_{tot}$) and progressive e-fold increases in the initial expectation value r_0^*. In Fig. 6 A, the effector lifetime τ_E is shorter; in Fig. 6 B it is longer than τ_{R^*}. The dotted horizontal line denotes again the criterion level. Of course, taking $E^+(t)$ into account delays the decline in effector activity. However, the space between the intersection of the curves for e-fold increases in r_0^* with the criterion line is only affected for small bleaches and only if $\tau_E > \tau_{R^*}$ (Fig. 6 B). For bleaches that initially elevate the effector activity to its maximum plateau level, the space between subsequent curves is still τ_{R^*}, which is not influenced by the value of τ_E, even if that is greater than τ_{R^*}. This contradicts the seemingly obvious interpretation that it is generally the longest lifetime of the transduction cascade that determines the slope of the saturation function. The figure demonstrates that the important determinant is the time of departure from the state with at least one R^* on each disc (which depends only on the lifetime of R^*). The effector decay on the empty discs just adds a constant delay to it, i.e., the saturation function as given by Eqs. 22 and 23 is shifted by that constant over most of its course. Appendix E further elaborates on the influence of the effector lifetime on the initial part of the saturation function, i.e., for the case $r_0^* < 1$. In this range, the respective greater lifetime indeed determines the slope of the saturation function, which must cause a change in its slope in the initial part of the lower branch if $\tau_E > \tau_{R^*}$. For an illustration, the insets of Fig. 6, A and B, show the lower branch of the saturation function, as it is derived from the space between subsequent effector activity curves given in these figures, opposed to the experimental data points and the course of the saturation function, without consideration of the nonzero effector lifetime. For $\tau_E < \tau_{R^*}$, the new slope is constant and equals τ_{R^*} (Fig. 6 A), whereas for $\tau_{E^*} > \tau_{R^*}$, it continuously changes from an initial τ_{E^*} to τ_{R^*} after approximately one logarithmic unit. The lack of such a specific effect in the experimental data would argue for $\tau_{E^*} < \tau_{R^*}$; however, the few available data points leave the field very much open to speculation here. More experimentation with emphasis on the range of low flash intensities would be required to settle this point.

DISCUSSION

In this study we propose an explanation for properties of the retinal rod response under saturating stimulation. The theory specifically explains the time the receptor cell stays in saturation until the response recovers. The time-ordered sequence of binding and activation of the enzyme and formation of the product, the phosphorylated receptor, together with the limited reaction space of the disc membrane, are the only entries of the model.

The model explains the observation that the saturation function is biphasic. The reasonable agreement of the resulting saturation curve with the experimental curve indicates that the rhodopsin kinase-dependent mechanism described here governs the recovery kinetics in the range of R_0^* considered (less than ~10% of the total rhodopsin content). One can anticipate, however, that, at higher bleachings, the limited amount of arrestin (Mangini and Pepperberg, 1988) and the limited rate of the retinol dehydrogenase-mediated reduction of the photolyzed chromophore all-*trans*-retinal (Palczewski et al., 1994) will come into play.

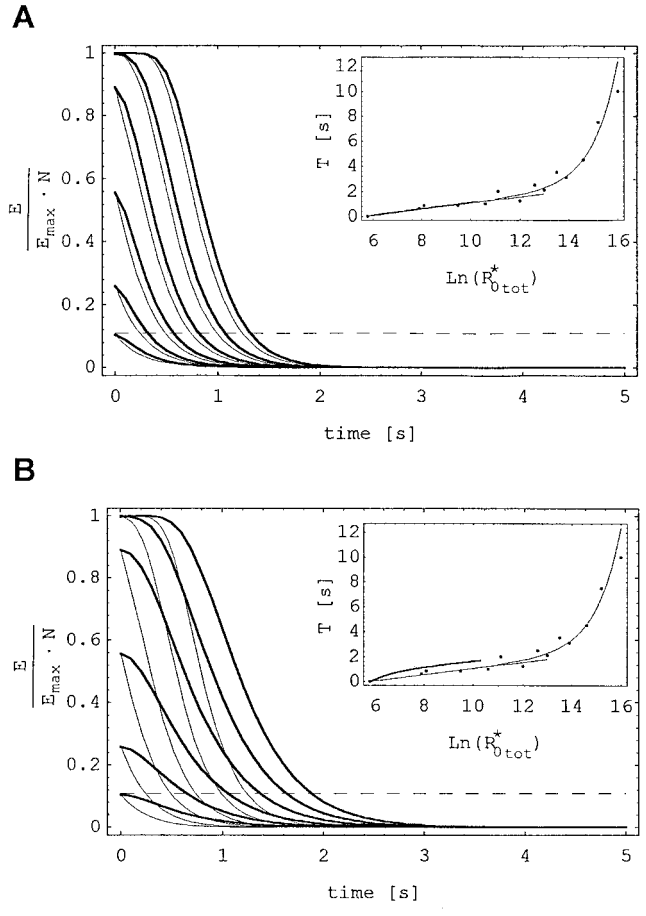

FIGURE 6 Comparison of the time course of normalized effector activity in the ROS for weak flashes with and without the contribution of the exponential effector decay on "empty discs." Thick lines, effector activity according to Eq. 28; thin lines, effector activity according to Eq. 15a. The broken horizontal line denotes again the criterion level. Subsequent curves are characterized by e-fold increases in r_0^*. $r_0^* = e^{5.8}/N, e^{6.8}/N, \ldots, e^{10.8}/N$). Parameters are as in Fig. 1; for the characteristic lifetime of the effector, a value of 0.07 s in *A* and 0.4 s in *B* was assumed. The insets show the experimental data points of the saturation function, the expressions for the two branches as given by Eqs. 22 and 23 (*thin lines*) and the course of the lower branch as it is derived from the space between the curves shown in the figure (*thick lines*).

Implicit in the current explanation are conclusions about a long-standing problem of visual excitation, namely the lifetime of active rhodopsin. The "innocent" question (Langlois et al., 1996), how long a given rhodopsin molecule, once activated, remains capable of activating the G-protein-coupled transduction cascade of the rod, is in fact a very tricky one. Not only is it necessary to distinguish between the intrinsic, characteristic lifetime of the free receptor and its real lifetime under conditions of steady engagement in complexes with G_t (in this case, R^* lives longer, and the lifetime distribution is distorted; Felber et al., 1996). More importantly, different approaches to the problem have led to different estimations:

1. For saturating numbers of R^* (>30 R^* per disc membrane), the estimation of the R^* lifetime, based on measurements of the saturation time, yields values on the order of 2 s (Pepperberg et al., 1992, 1996).

2. For single R^*, stochastic simulations (Felber et al., 1996) and electrophysiological (Chen et al., 1995) and heat production (Langlois et al., 1996) experiments suggest that the decay of R^* limits the rise of the response, which means much shorter R^* lifetimes (on the order of 0.3 s).

Our model explains the seeming conflict satisfyingly. For low bleachings, the rate of binding of rhodopsin to the kinase is determined by the thermodynamic properties of the complex only, whereas for larger bleachings that bring along substrate saturation of the enzyme, the phosphorylation reactions that precede the release of the enzyme become the pacemaker of the enzymatic turnover.

It is important to note that, in the framework of our model, the concept of a characteristic lifetime of active rhodopsin (which is defined as the time it takes for the pool of active rhodopsin to decline to $1/e$ of its initial value) becomes relatively meaningless for strong bleaches. In that case, the linear component in the temporal evolution of R^* given by Eq. 6 outweighs the exponential one, and thus the characteristic lifetime is not constant but depends on R_0^*.

Although the data mentioned so far are nicely consistent with our model, it is confronted with a criticism that applies to every model that describes the decline of active rhodopsin for weak bleaches by first-order kinetics. In the single quantum regime, the rod response is relatively uniform, i.e., it does not vary more than 20% for single quantum excitation (Baylor et al., 1984). These data impose a rigid condition on every model of signal transduction. The exponential lifetime distribution for active rhodopsin that results from first-order deactivation kinetics might cause a large stochastic variability of the response. However, a study by Felber et al. (1996) has shown that already on the level of phosphodiesterase activity, the variability in the time course that results from exponential R^* decay, even when it occurs during the rise of the response, is surprisingly small because of the intrinsic "kinetic buffer" effect of the amplifying cascade.

Furthermore, we assumed that none of the states of rhodopsin that follow the binding of the kinase was active. In fact, phosphorylated rhodopsin maintains a certain transducin-activating capacity ((Dodd et al., 1996); (Miller et al., 1986)). Because the replacement of the kinase with arrestin takes time, in this break the recovery would be interrupted. We justified this simplification with the fast binding of arrestin (Hofmann et al., 1995; Pulvermüller et al., 1997).

The current version of the model contains two special assumptions, namely

1. The size and number of discs (and their kinase content) were chosen according to data from warm-blooded animals.

2. Rhodopsin kinase binding (before any action of the phosphate donor ATP) is sufficient to inhibit the binding and catalytic activation of the G-protein (Pulvermüller et al., 1993).

Both assumptions shape the simulated saturation function but are not mandatory for the model to apply. Assuming

larger discs with accordingly higher rhodopsin kinase content, like the ones found in salamander rods, will lead to characteristic diffences in the calculated saturation function. It can be predicted that the onset of the upper branch (the onset of enzyme saturation) will be shifted to higher R^*, leaving a quasilinear saturation function, in agreement with the experimental data from this organism (Pepperberg et al., 1992). If other mechanisms of receptor kinase/G-protein interdependence are assumed, as for example, that binding of the G-protein $\beta\gamma$-subunit, once separated from the α-subunit after G-protein activation, is required to activate receptor kinase (see Helmreich and Hofmann, 1996, for a discussion), related but adequately adapted models have to be applied.

APPENDIX A

In this section, the quasi-steady-state (QSS) approximation for the kinetic equations in Eq. 1a for small values of the characteristic ratio φ is derived. By introducing the normalized variables τ, ρ, and κ, the normalized parameter λ,

$$\tau = t \cdot k_1 \cdot RK_{\text{tot}}, \quad \rho = \frac{R^*}{R_0^*}, \quad \kappa = \frac{R^*RK}{RK_{\text{tot}}}, \quad \lambda = \frac{k_2}{k_1 \cdot R_0^*} \tag{A1}$$

and the parameter φ as defined in Eq. 2,

$$\varphi = \frac{R_0^*}{RK_{\text{tot}}}$$

the differential equation system in Eq. 1a can be transformed to

$$\begin{aligned} \frac{d\rho}{d\tau} &= -(1-\kappa)\cdot\rho \\ \frac{d\kappa}{d\tau} &= \frac{1}{\varphi}\cdot((1-\kappa)\cdot\rho - \lambda\cdot\kappa) \end{aligned} \tag{A2}$$

If $\varphi \ll 1$, it is obvious from the second equation that the change in κ is much faster than the change in ρ. This allows us to assume that κ will always be able to reach a quasi-steady state, i.e., a balance with the momentary ρ value that is given by

$$\kappa \approx \frac{\rho}{\lambda + \rho} \tag{A3}$$

Using this expression, the first equation, back in unnormalized form, reads

$$\frac{dR^*}{dt} = -\frac{k_2 \cdot RK_{\text{tot}} \cdot R^*}{k_2/k_1 + R^*} \tag{A4}$$

which is the approximation for small φ that is used in Eq. 4.

For a more detailed treatment of the QSS approach, we refer to Heinrich and Schuster (1996).

APPENDIX B

The initial distribution of the R^*'s among the disc membranes is Poissonian, because the probability of a single event—a photon hitting one particular disc—is very small, but the overall number of events is large—the flash delivers numerous photons at the ROS. The question is whether the distribution of the R^* at later times can still be described as Poissonian, because the number of R^* changes individually on each disc membrane according to a defined time law.

Let the R^* be Poisson distributed among the disc membranes at time t:

$$P_{\text{k}}(t) = \frac{r^*(t)^{\text{k}}}{k!}\cdot e^{-\text{r}^*(\text{t})} \tag{B1}$$

where $P_{\text{k}}(t)$ stands for the probability of finding k R^* on a disc membrane, and $r^*(t)$ for the expectation value of the number of R^* on a disc membrane at time t. Now consider the temporal evolution of this distribution. The master equation provides an expression for the change in the probability $P_{\text{k}}(t)$:

$$\frac{dP_{\text{k}}(t)}{dt} = P_{\text{k}+1}(t)\cdot f(k+1) - P_{\text{k}}(t)\cdot f(k) \tag{B2}$$

where $f(k)$ denotes the transition rate, that is the rate at which a disc membrane occupied by k R^* transforms into one that is occupied by $k-1$ R^*:

$$\frac{dk}{dt} = -f(k) \tag{B3}$$

If the probability distribution remains Poissonian, then the change in each probability $P_{\text{k}}(t)$ depends only on the change of the expectation value:

$$\begin{aligned} \frac{dP_{\text{k}}(t)}{dt} &= \frac{d}{dt}\left(\frac{r^*(t)^{\text{k}}}{k!}\cdot e^{-\text{r}^*(\text{t})}\right) \\ &= \frac{r^*(t)^{\text{k}}}{k!}\cdot e^{-\text{r}^*(\text{t})}\cdot\left(\frac{k}{r^*(t)} - 1\right)\cdot\bar{f}(r^*) \end{aligned} \tag{B4}$$

with

$$\frac{dr^*}{dt} = -\bar{f}(r^*) \tag{B5}$$

denoting the rate at which the expectation value changes. If the individual change in the R^* number on each disc membrane does not alter the Poisson fashion of the distribution of the R^* among the disc membranes, then Eqs. B2 and B4 have to be equal and the condition for conservation of the Poisson distribution reads

$$r^*\cdot\frac{f(k+1)}{k+1} - f(k) = \bar{f}(r^*) - k\cdot\frac{\bar{f}(r^*)}{r^*} \tag{B6}$$

For example, rates f and $\bar{f}$ that are both linear in k (resp. r^*) with equal slope would fulfill the condition given in Eq. B6 for all k; equal constant (zero order) rates f and $\bar{f}$ would fail to fulfill it.

APPENDIX C

In this section, expressions for the transition rates in Eq. B3 are derived. The master equation approach for the change in probability that a disc membrane contains k R^* and i R^*RK reads

$$\begin{aligned} \frac{dP_{\text{k,i}}}{dt} &= k_1\cdot(RK_{\text{tot}} - (i-1))\cdot(k+1)\cdot P_{\text{k}+1,\text{i}-1} - k_1 \\ &\quad\cdot(RK_{\text{tot}} - i)\cdot k\cdot P_{\text{k,i}} + k_2\cdot(i+1) \\ &\quad\cdot P_{\text{k,i}+1} - k_2\cdot i\cdot P_{\text{k,i}} \end{aligned} \tag{C1}$$

Uncoupling the probabilities according to

$$P_{\text{k,i}} \approx P_{\text{k}}\cdot P_{\text{i}} \tag{C2}$$

and uncoupling the master equations via summing the right-hand side of Eq. C1 over all possible values of the respective other variable leads to one equation for each of the two uncoupled probabilities that depends on the expectation value of the other variable:

$$\frac{dP_k}{dt} = k_1 \cdot (RK_{tot} - r^*rk(t)) \cdot ((k+1) \cdot P_{k+1} - k \cdot P_k) \quad \text{(C3)}$$

$$\frac{dP_i}{dt} = k_1 \cdot r^*(t) \cdot ((RK_{tot} - (i-1)) \cdot P_{i-1} - (RK_{tot} - i) \cdot P_i) + k_2 \cdot ((i+1) \cdot P_{i+1} - i \cdot P_i) \quad \text{(C4)}$$

The same principles that allow simplification of the macroscopic deterministic kinetic equations depending on the value of φ in Eq. 2 now enable us to rewrite and simplify the equations for the temporal evolution of the probabilities depending on the value of its stochastic analogon,

$$\bar{\varphi} = \frac{RK_{tot}}{r^*(0)} \quad \text{(C5)}$$

For large $\bar{\varphi}$ the expectation value $r^*rk(t)$, which cannot be greater than $r^*(0)$, becomes negligible compared to RK_{tot}, and Eq. C3 can be approximated by

$$\left.\frac{dP_k}{dt}\right|_{\bar{\varphi}\gg 1} \approx k_1 \cdot RK_{tot} \cdot ((k+1) \cdot P_{k+1} - k \cdot P_k) \quad \text{(C6)}$$

For small $\bar{\varphi}$ it can be shown that a quasistationary probability distribution for the R^*RK evolves. Quasistationary means stationary with respect to the expectation value $r^*(t)$, which changes relatively slowly. The mathematical formalism of extracting the small parameter on the left-hand side of the equation was demonstrated in Appendix A and results in:

$$\bar{\varphi} \cdot \left.\frac{dP_i}{d\tau}\right|_{\bar{\varphi}\ll 1} \approx 0 = \frac{r^*(t)}{r^*(0)} \cdot ((RK_{tot} - (i-1)) \cdot P_{i-1}(t) - (RK_{tot} - i) \cdot P_i(t)) + \gamma \cdot ((i-1) \cdot P_{i-1}(t) - i \cdot P_i(t)) \quad \text{(C7)}$$

with $\tau = t \cdot k_1 \cdot RK_{tot}$ and $\gamma = k_2/(k_1 \cdot r^*(0))$.

Using $P_{i>RK_{tot}} = 0$, we can determine all probabilities P_i from the value of $P_{RK_{tot}}$:

$$P_{RK_{tot}-n} = \frac{\gamma^n \cdot \prod_{x=0}^{n-1}(RK_{tot} - x)}{n! \cdot (r^*(t)/r^*(0))^n} \cdot P_{RK_{tot}} = \binom{RK_{tot}}{RK_{tot} - n} \cdot \left(\frac{\gamma \cdot r^*(0)}{r^*(t)}\right)^n \cdot P_{RK_{tot}} \quad \text{(C8)}$$

For a binomial distribution,

$$P_{m-n} = \binom{m}{m-n} \cdot p^{m-n} \cdot (1-p)^n = \binom{m}{m-n} \cdot p^m \cdot \left(\frac{1}{p} - 1\right)^n = \binom{m}{m-n} \cdot \left(\frac{1}{p} - 1\right)^n \cdot p_m \quad \text{(C9)}$$

holds. Comparison of Eqs. C8 and C9 reveals that the quasistationary probability distribution is binomial with the single event probability (i.e., the probability that a molecule of kinase is bound to R^*):

$$p = \frac{r^*(t)}{k_2/k_1 + r^*(t)} \quad \text{(C10)}$$

and the expectation value

$$r^*rk(t) = RK_{tot} \cdot \frac{r^*(t)}{k_2/k_1 + r^*(t)} \quad \text{(C11)}$$

Introducing Eq. C11 in Eq. C3 leads to

$$\left.\frac{dP_k}{dt}\right|_{\bar{\varphi}\ll 1} \approx \frac{k_2 \cdot RK_{tot}}{k_2/k_1 + r^*(t)} \cdot ((k+1) \cdot P_{k+1}(t) - k \cdot P_k(t)) \quad \text{(C12)}$$

Equations C6 and C12 contain the desired approximations for the transition rates f in Eq. B3 for initial conditions that are distinguished by large (resp. small) values of $\bar{\varphi}$.

APPENDIX D

In this section, expressions for the expectation value kinetics in Eq. B5 are derived. With

$$\frac{dr^*(t)}{dt} = \sum_{k=0}^{R^*_{0_{tot}}} k \cdot \frac{dP_k}{dt} \quad \text{(D1)}$$

and Eqs. C6 (resp. C12), the following expressions for the temporal evolution of the expectation value can be found:

$$\left.\frac{dr^*(t)}{dt}\right|_{\bar{\varphi}\gg 1} \approx k_1 \cdot RK_{tot} \cdot \sum_{k=0}^{R^*_{0_{tot}}} k \cdot (k+1) \cdot P_{k+1}(t) - k^2 \cdot P_k(t) = k_1 \cdot RK_{tot} \cdot \sum_{k=0}^{R^*_{0_{ges}}} [(k+1)^2 \cdot P_{k+1} - (k+1) \cdot P_{k+1} - k^2 \cdot P_k] = -k_1 \cdot RK_{tot} \cdot r^*(t) \quad \text{(D2)}$$

and

$$\left.\frac{dr^*(t)}{dt}\right|_{\bar{\varphi}\ll 1} \approx \frac{k_2 \cdot RK_{tot}}{k_2/k_1 + r^*(t)} \cdot \sum_{k=0}^{R^*_{0_{tot}}} [k \cdot (k+1) \cdot P_{k+1} - k^2 \cdot P_k] = -\frac{k_2 \cdot RK_{tot}}{k_2/k_1 + r^*(t)} \cdot r^*(t) \quad \text{(D3)}$$

It is reassuring to find that the equations for the temporal evolution of the expectation value (Eqs. D2 and D3) that were derived with the stochastic approach are indeed identical to the macroscopic kinetic equations (Eqs. 3 and 4).

Introducing the transition rates from Eqs. C6 and C12 and the expectation value kinetics (Eqs. D2 and D3) into Eq. B6 shows that the condition for conservation of the Poissonian character of the distribution of the R^* among the disc membranes for all times is fulfilled for great and small $\bar{\varphi}$.

APPENDIX E

The integral in Eq. 27 can be solved by expanding $dP_{R^*=0}(\tau)$:

$$dP_{R^*=0}(\tau) = -\frac{1}{2}\frac{dr^*}{d\tau}\cdot e^{-r^*/2} = \frac{1}{2}\cdot\left(-\frac{dr^*}{d\tau}\right)\cdot\left(1-\frac{r^*}{2}+\frac{1}{2}\left(\frac{r^*}{2}\right)^2-\frac{1}{6}\left(\frac{r^*}{2}\right)^3+\ldots\right). \quad \text{(E1)}$$

With

$$r^* = r_0^*\cdot e^{-(\tau/\tau_{R^*})},$$

the solution of Eq. 27 is found in the form of an infinite row:

$$E^+(t) = N\cdot E_{max}\cdot\sum_{n=1}^{\infty}\left[(-1)^{n-1}\frac{n\cdot\tau_E}{\tau_{R^*}-n\cdot\tau_E}\cdot\frac{1}{n!}\left(\frac{r_0^*}{2}\right)^n\cdot\left(e^{-n\cdot t/\tau_{R^*}}-e^{-t/\tau_E}\right)\right] \quad \text{(E2)}$$

If $\tau_{R^*} = n\cdot\tau_E$, the nth element of the sum

$$(-1)^{n-1}\cdot\frac{n\cdot\tau_E}{\tau_{R^*}-n\cdot\tau_E}\cdot\frac{1}{n!}\cdot\left(\frac{r_0^*}{2}\right)^n\cdot\left(e^{-n\cdot t/\tau_{R^*}}-e^{-t/\tau_E}\right)$$

is replaced by

$$(-1)^{n-1}\cdot\frac{1}{n!}\cdot\left(\frac{r_0^*}{2}\right)^n\cdot\frac{t}{\tau_E}.$$

By introducing Eq. 15a, also in its expanded form, Eq. 28 can be written as

$$E_{tot}(t) = N\cdot E_{max}\cdot\sum_{n=1}^{\infty}(-1)^{n-1}\cdot\frac{\tau_{R^*}}{\tau_{R^*}-n\cdot\tau_E}\cdot\left(\frac{r_0^*}{2}\right)^n\cdot\frac{1}{n!}\cdot e^{-n\cdot t/\tau_{R^*}} + N\cdot E_{max}\cdot e^{-t/\tau_E}\cdot\sum_{n=1}^{\infty}(-1)^n\cdot\frac{n\cdot\tau_E}{\tau_{R^*}-\tau_E}\cdot\left(\frac{r_0^*}{2}\right)^n\frac{1}{n!} \quad \text{(E3)}$$

For the case of initial values r_0^* smaller than 1, both τ_{R^*} and τ_{E^*} influence the saturation time. For $r_0^* \ll 1$, higher order terms in Eq. E2 can be neglected, which leads to an approximation for Eq. E3:

$$E_{tot}(t) \approx N\cdot E_{max}\cdot\frac{r_0^*}{2}\cdot\left(\frac{\tau_{R^*}}{\tau_{R^*}-\tau_E}\cdot e^{-t/\tau_{R^*}}-\frac{\tau_E}{\tau_{R^*}-\tau_E}\cdot e^{-t/\tau_E}\right) \quad \text{(E4)}$$

Note the symmetry in the expression. For $\tau_{R^*} \gg \tau_{E^*}$ or vice versa, it is the respective dominating time constant that determines the space between intersections of curves with the criterion line for e-fold increases in r_0^*. For intermediate cases, the space between the intersections is influenced by both time constants.

We thank Stefan Felber, David Pepperberg, and David Schneeweis for discussions. David Schneeweis kindly provided us with experimental data before their publication.

Financial support from the Deutsche Forschungsgemeinschaft is gratefully acknowledged.

REFERENCES

Baylor, D. A., B. J. Nunn, and J. L. Schnapf. 1984. The photocurrent, noise and spectral sensitivity of rods of the monkey *Macaca fascicularis*. *J. Physiol. (Lond.).* 357:575–607.

Birch, D. G., D. C. Hood, S. Nusinowitz, and D. R. Pepperberg. 1995. Abnormal activation and inactivation mechanisms of rod transduction in patients with autosomal dominant retinitis pigmentosa and the pro-23-his mutation. *Invest. Ophthalmol. Vis. Sci.* 35:1603–1614.

Chen, J., C. L. Makino, N. S. Peachey, D. A. Baylor, and M. I. Simon. 1995. Mechanisms of rhodopsin inactivation in vivo as revealed by a COOH-terminal truncation mutant. *Science.* 267:374–377.

Dean, K. R., and M. Akhtar. 1996. Novel mechanism for the activation of rhodopsin kinase: implications for other G protein-coupled receptor kinases (GRK's). *Biochemistry.* 35:6164–6172.

Dodd, R. L., C. L. Makino, J. Xu, J. Chen, M. I. Simon, and D. A. Baylor. 1996. Knockout of arrestin delays final shut-off of the rod photoresponse. *Invest. Ophthalmol. Vis. Sci.* 37, 85

Felber, S., H. P. Breuer, F. Petruccione, J. Honerkamp, and K. P. Hofmann. 1996. Stochastic simulation of the transducin GTPase cycle. *Biophys. J.* 71:3051–3063.

Heinrich, R., and St. Schuster. 1996. The quasi-steady-state approximation. *In* The Regulation of Cellular Systems. Chapman and Hall, New York. 116–123.

Helmreich, E. M., and K. P. Hofmann. 1996. Structure and function of proteins in G-protein coupled signaltransfer from receptor to effector: a comparison of visual and hormonal signaltransduction. *Biochim. Biophys. Acta.* 1286:285–322.

Hofmann, K. P., and M. Heck. 1996. Light-induced protein-protein interactions on the rod photoreceptor disc membrane. *In* Biomembranes II. A. G. Lee, editor. JAI Press, Greenwich, CT.

Hofmann, K. P., S. Jäger, and O. P. Ernst. 1995. Structure and function of activated rhodopsin. *Isr. J. Chem.* 35:339–355.

Inglese, J. N., J. Freedman, W. J. Koch, and R. J. Lefkowitz. 1993. Structure and mechanism of the G protein-coupled receptor kinases. *J. Biol. Chem.* 32:23735–23738.

Lagnado, L., and D. A. Baylor. 1992. Signal flow in visual transduction. *Neuron.* 8:995–1002.

Lamb, T. D. 1994. Stochastic simulation of activation in the G-protein cascade of phototransduction. *Biophys. J.* 67:1439–1454.

Lamb, T. D., and E. N. Pugh, Jr. 1992. A quantitative account of the activation steps involved in phototransduction in amphibian photoreceptors. *J. Physiol. (Lond.).* 449:719–758.

Langlois, G., C. K. Chen, K. Palczewski, J. B. Hurley, and T. M. Vuong. 1996. Responses of the phototransduction cascade to dim light. *Proc. Natl. Acad. Sci. USA.* 93:4677–4682.

Lyubarsky, A. L., and E. N. Pugh, Jr. 1996. Recovery phase of the murine rod photoresponse reconstructed from electroretinographic recordings. *J. Neurosci.* 16:563–5671.

Mangini, N. L., and D. R. Pepperberg 1988. Immunolocalization of 48K in rod photoreceptors—light and ATP increase OS labeling. *Invest. Ophthalmol. Vis. Sci.* 92:1221–1234.

Miller, J. L., D. A. Fox, and B. J. Litman. 1986. Amplification of phosphodiesterase activation is greatly reduced by rhodopsin phosphorylation. *Biochemistry.* 25:4983–4988.

Palczewski, K. 1997. GTP-binding protein-coupled receptor kinases: two mechanistic models. *Eur. J. Biochem.* 248:261–269.

Palczewski, K., S. Jager, J. Buczylko, R. K. Crouch, D. L. Bredberg, K. P. Hofmann, M. A. Asson Batres, and J. C. Saari. 1994. Rod outer segment retinol dehydrogenase: substrate specificity and role in phototransduction. *Biochemistry.* 33:13741–13750.

Pepperberg, D. R., D. G. Birch, K. P. Hofmann, and D. C. Hood. 1996. Recovery kinetics of human rod phototransduction inferred from the two-branched a-wave saturation function. *J. Opt. Soc. Am. A.* 13: 586–600.

Pepperberg, D. R., M. C. Cornwall, M. Kahlert, K. P. Hofmann, J. Jin, G. J. Jones, and H. Ripps. 1992. Light-dependent delay in the falling phase of the retinal rod photoresponse. *Vis. Neurosci.* 8:9–18.

Pepperberg, D. R., M. Kahlert, A. Krause, and K. P. Hofmann. 1988. Photic modulation of a highly sensitive, near-infrared light-scattering

signal recorded from intact retinal photoreceptors. *Proc. Natl. Acad. Sci. USA.* 85:5531–5535.

Pugh, E. N., Jr., and T. D. Lamb. 1990. Cyclic GMP and calcium: the internal messengers of excitation and adaptation in vertebrate photoreceptors. *Vision Res.* 30:1923–1948.

Pulvermüller, A., D. Maretzki, M. Rudnicka-Nawrot, W. C. Smith, K. Palczewski, and K. P. Hofmann. 1997. Functional differences in the interaction of arrestin and its splice variant, p^{44}, with rhodopsin. *Biochemistry.* 36:9253–9260.

Pulvermüller, A., K. Palczewski, and K. P. Hofmann. 1993. Interaction between photoactivated rhodopsin and its kinase: stability and kinetics of complex formation. *Biochemistry.* 32:14082–14088.

Schleicher, A., H. Kühn, and K. P. Hofmann. 1989. Kinetics, binding constant, and activation energy of the 48-kDa protein-rhodopsin complex by extra-metarhodopsin II. *Biochemistry.* 28:1770–1775.

Schneeweis, D. M., and J. L. Schnapf. 1995. Photovoltage of rods and cones in the macaque retina. *Science.* 268:1053–1056.

Vuong, T. M., M. Chabre, and L. Stryer. 1984. Millisecond activation of transducin in the cyclic nucleotide cascade of vision. *Nature.* 311: 659–661.

Wilden, U., S. W. Hall, and H. Kühn. 1986. Phosphodiesterase activation by photoexcited rhodopsin is quenched when rhodopsin is phosphorylated and binds the intrinsic 48-kDa protein of rod outer segments. *Proc. Natl. Acad. Sci. USA.* 83:1174–1178.